International Journal for Parasitology: Drugs and Drug Resistance 20 (2022) 97–107

Contents lists available at ScienceDirect

International Journal for Parasitology: Drugs and Drug Resistance

journal homepage: www.elsevier.com/locate/ijpddr

Uncovering the antimalarial potential of toad venoms through a bioassay-guided fractionation process

Mathilde Wells [a], Mathieu Fosséprés [b], Stéphanie Hambye [a], Mathieu Surin [b], Bertrand Blankert [a,*]

[a] Laboratory of Pharmaceutical Analysis, Faculty of Medicine and Pharmacy, Research Institute for Health Sciences and Technology, University of Mons - UMONS, Place du Parc 20, 7000, Mons, Belgium

[b] Laboratory for Chemistry of Novel Materials, Faculty of Sciences, Research Institute for Biosciences and Research Institute for Materials, University of Mons - UMONS, Place du Parc 20, 7000, Mons, Belgium

ARTICLE INFO

Keywords:
Malaria
Rhinella marina
Bufadienolide
Toad venom
Separative techniques

ABSTRACT

Malaria remains to date one of the most devastating parasitic diseases worldwide. The fight against this disease is rendered more difficult by the emergence and spread of drug-resistant strains. The need for new therapeutic candidates is now greater than ever. In this study, we investigated the antiplasmodial potential of toad venoms. The wide array of bioactive compounds present in *Bufonidae* venoms has allowed researchers to consider many potential therapeutic applications, especially for cancers and infectious diseases. We focused on small molecules, namely bufadienolides, found in the venom of *Rhinella marina (L.)*. The developed bio-guided fractionation process includes a four solvent-system extraction followed by fractionation using flash chromatography. Sub-fractions were obtained through preparative TLC. All samples were characterized using chromatographic and spectrometric techniques and then underwent testing on *in vitro Plasmodium falciparum* cultures. Two strains were considered: 3D7 (chloroquine-sensitive) and W2 (chloroquine-resistant). This strategy highlighted a promising activity for one compound named resibufogenin. With IC_{50} values of (29 ± 8) μg/mL and (23 ± 1) μg/mL for 3D7 and W2 respectively, this makes it an interesting candidate for further investigation. A molecular modelling approach proposed a potential binding mode of resibufogenin to *Plasmodium falciparum* adenine-triphosphate 4 pump as antimalarial drug target.

1. Introduction

Malaria is a parasitic disease caused by several species of *Plasmodium* protozoans. The main mode of transmission is through the bite of infected female *Anopheles* mosquitoes. Five species are known to infect humans: *P. falciparum*, *P. vivax*, *P. ovale*, *P. malariae* and *P. knowlesi*. *Plasmodium falciparum* (*Pf*) is the most prevalent species in the sub-Saharan regions and is also the species responsible for most deaths and the most likely to lead to severe forms of the infection such as cerebral malaria. Malaria remains to date one of the deadliest infectious diseases in the world, claiming mostly children under 5-years-old as its victims (77% of all malaria deaths) (World Health Orgnization (WHO) 2021; Phillips et al., 2017).

In 2020, the World Health Organization (WHO) reported 241 million cases and approximately 647,000 deaths. These figures have risen since 2019 partly due to the various disruptions caused by the COVID-19 pandemic (World Health Orgnization (WHO) 2021). Moreover, the emergence and spread of drug-resistant strains remains a constant hindrance to the efforts to control and eliminate this endemic disease. Most established antimalarial drugs are concerned by this phenomenon, such as quinine, chloroquine, sulfadoxine-pyremethamine among others. The most common drug resistance-associated genes identified for *P. falciparum* are *Pfcrt* (chloroquine resistance transporter), *Pfmdr1* (multi-drug resistance protein 1), *Pfcytb* (atovaquone), *Pfdhps* (type 1 antifolates such as sulfonamides and sulfones) and *Pfdhfr* (type 2 antifolates such as pyrimethamine) (Arya et al., 2021; Kumar et al., 2018; Olliaro 2001). To reduce the risk of resistances developing, the WHO guidelines exclusively recommend the use of Artemisinin-based Combination Therapy (ACT) as first-line of treatment. However, artemisinin-resistant strains have been reported and have started spreading across Southeast Asia and some parts of Africa. The *PfK13* gene (Kelch protein 13) is responsible for resistances to artemisinin and its derivates (Tilley et al., 2016; Kobasa et al., 2018; Boussaroque et al., 2016; Kagoro et al., 2022). The multiplication of these mutant strains

* Corresponding author.
E-mail address: bertrand.blankert@umons.ac.be (B. Blankert).

https://doi.org/10.1016/j.ijpddr.2022.10.001
Received 10 May 2022; Received in revised form 16 September 2022; Accepted 7 October 2022
Available online 14 October 2022

will most certainly lead to an increase in treatment failures which in turn will give way to a rise in mortality rates. The WHO is constantly updating its guidelines and the need for new therapeutic candidates with novel targets is now a priority more than ever.

Natural products are familiar candidates in the field of antimalarial drug discovery. The best-known examples are quinine and artemisinin and their respective synthetic derivates. Quinine is an alkaloid that was isolated from the bark of the *Cinchona* genus for the first time in 1820. Artemisinin was discovered later in the 1970s by Tu Youyou (Tu 2011). Artemisinin is a sesquiterpene lactone found in *Artemisia annua*, a plant widely used in *Chinese* medicine. Plants have always been and continue to be a great source of therapeutically active compounds (Tajuddeen and Van Heerden 2019; Atanasov et al., 2021; Wells 2011). However, over the years, animal venoms and secretions have been at the center of an ever-growing interest in the field of drug discovery. Indeed, some venoms led to the discovery of active compounds, either proteins or small molecules, which in turn were made into well-known drugs (e.g., Captopril® from the snake *Bothrops jararaca*, Exenatide from the *Gila monster*, etc.) (King 2011; Harvey 2014; Utkin 2015). Another interesting yet relatively unexplored area are the venoms and secretions produced by toads. For centuries, the skins and secretions from amphibians have been used in traditional medicine (e.g., *Chan'su*) (Wei et al., 2020; Chen et al., 2015). Many therapeutic activities can be associated to these venoms: antimicrobial (*E. coli*), antiviral (HIV), cytotoxic (lead for potential anticancer drugs), analgesic and anesthetic among others (Rodríguez et al., 2017). Recent reports have also highlighted antiparasitic properties and more interestingly so antiplasmodial activities. These studies mainly focused on frog venoms and their peptidic content. The main peptides that displayed a potential antiplasmodial activity are phylloseptins and dermaseptins both found in the cutaneous secretions of the *Phyllomedusa* genus (Liu et al., 2020; Rivas et al. 2009; Krugliak et al., 2000; Ghosh et al., 1997; Dagan et al., 2002; Kückelhaus et al., 2009). However, a couple of these papers put forward the use of small molecules, namely bufadienolides, isolated from the venom of toads as potential antiplasmodial compounds (Banfi et al., 2016; Medeiros et al., 2019).

Bufadienolides are part of the cardiotonic steroid (CTS) family. They can be naturally sourced in plants of various families (*Francoaceae*, *Crassulaceae*, *Ranunculaceae*, etc.) and in some animals among which a species of firefly and even a species of *Rhabdophis* snakes (Bedane et al., 2020; Kolodziejczyk-Czepas et al., 2018; Iguchi et al., 2020). However, their main exogenous sources are the parotoid glands and skin secretions of various *Bufonidae* species (e.g., *Rhinella marina*, *Bufo bufo gargarizans*, *Bufo melanostictus*) (Krenn and Kopp 1998; Rodríguez et al., 2017). In many toad venoms, they represent the main constituents alongside other compounds such as alkaloids, peptides and proteins and biogenic amines occurring in smaller proportions. As shown in Fig. 1, bufadienolide compounds are characterized by a common steroid-core structure. Bufadienolides (C_{24}) possess a δ-lactone ring in the C_{17} position in the β orientation. In the *Bufonidae* family, CTS are present as two forms, free and conjugated. Free forms are also known as bufagins (*e.g.,* marinobufagenin, etc.) and conjugated forms as bufotoxins. The latter are esterified at the C_3 position with a polar moiety, in the form of either an amino acid, a carboxylic acid or a sulfate group linked to a dicarboxylic acid. Among these, the most frequently occurring are amino acids-dicarboxylic acid couplings (e.g., marinobufotoxin, etc.) (Pavlovic 2014, 2020; Bagrov et al. 2009).

Physiologically, bufadienolides act by binding to the Na^+/K^+-ATPase pump (NKA), a ubiquitous ATP-dependent transport enzyme. Their primary function is to maintain and tune the ion gradient across the cell membrane by pumping, at the same time, three sodium ions outside and two potassium ions inside the cell (Bagrov et al. 2009; Toyoshima et al. 2011; Schoner 2002). *Pf* expresses a series of ATP-dependent pumps, among which the *Plasmodium falciparum* adenine-triphosphate 4 pump (*PfATP4*). The cation ATPase *Pf* P-type ATP_4 helps maintain the parasites Na^+ homeostasis through Na^+ ions efflux accompanied by an influx of H^+. The inhibition of this pump leads to an accumulation of Na^+ within the parasitophorous vacuole that could disrupt the finely tuned ion equilibrium of the parasites and lead to their death (Spillman and Kirk, 2015; Spillman et al., 2013; Flannery et al., 2015; Dick et al. 2020; Gilson et al., 2019).

In this work, we investigated the possibility that bufadienolides, based on their primary binding mechanisms to the Na^+/K^+-ATPase pump, could potentially bind to *PfATP4* and lead to toxicity for the parasites.

To this aim, we identified potential antiplasmodial candidates by developing a systematic bioassay-guided fractionation process. This strategy combines various analytical and separative tools, among which flash chromatography that is rarely applied to the fractionation of toad venom extracts (Kamalakkannan et al., 2017). The antiplasmodial

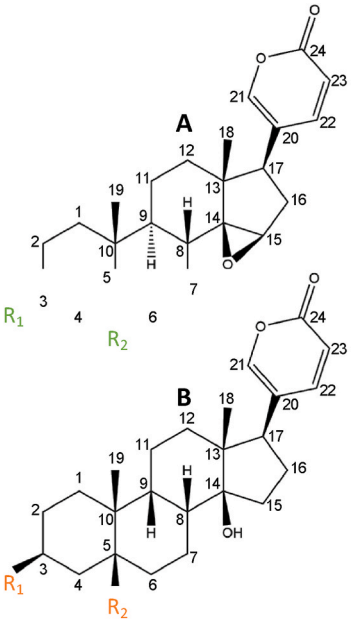

A – Epoxy group in C_{14}-C_{15}

	R_1	R_2
Marinobufagenin	-OH	-OH
Resibufogenin	-OH	-H
Marinobufotoxin	$-OCO(CH_2)_6COArg$	-OH

B – No epoxy group in C_{14}-C_{15}

	R_1	R_2
Telocinobufagin	-OH	-OH
Bufalin	-OH	-H
Telocinobufotoxin	$-OCO(CH_2)_6COArg$	-OH

Fig. 1. Chemical structures of the most common bufadienolides isolated from *Bufonidae* venoms.

activity was studied *in vitro*. For this purpose, two *Pf* strains have been selected: a chloroquine-sensitive strain (3D7) and a chloroquine-resistant one (W2). We focused on the asexual blood stage. Samples displaying sufficient antiplasmodial activity are assessed for their toxicity on normal human cell lines and on human red blood cells (RBCs). This paper discusses the bio-guided fractionation of *Rhinella marina (L.)* (*RM*) venom but the process can be transferred to other toad species. We will also study the potential binding modes of one of these candidates to the novel antimalarial drug target (*PfATP4*) through molecular modeling.

2. Material and methods

2.1. General experimental procedures

NMR spectra were acquired using a Bruker 600 MHz spectrometer at room temperature. HRMS spectra were acquired on a Waters Q-ToF US (Waters®, Milford, CT, USA) in ESI positive mode (capillary voltage 3.1 kV, source temperature 80 °C, collision energy 30 V). HPLC-UV/MS analyses were performed on an Agilent Technologies 1260 Infinity II system, equipped with a 1260 Quat VL pump and a 1260 WR DAD detector. The HPLC system was coupled to an Advion Expression CMS simple quadrupole (Advion, Ithaca, USA) (ESI voltage 3.5 kV, source temperature 200 °C, cone voltage 20 V). Flash chromatography was performed using the puriFLASH 215 system, equipped with a quaternary pump, UV and Evaporative Light Scattering detectors (Interchim, Montluçon, France). Samples were deposit on the TLC plates (Silica-gel 60 F_{254} HPTLC grade, Merck, Darmstadt, Germany) by an automated TLC sampler (Camag® Automatic Sampler 4, Switzerland). The migration was performed in an automated developing chamber (Camag® Automatic Developing Chamber 2, Switzerland). Plates were visualized using the Camag® TLC Visualizer 2. Microplates were read using the SpectraMax® M2 (Molecular Devices, San Jose, CA, USA). All solvents used for the extraction and fractionation, HPLC and TLC analyses were of analytical grade (Chem-Lab n.v., Zedelgem, Belgium). Reference standards for four bufadienolides were supplied. Marinobufagenin and telocinobufagin were purchased from Musechem® (New Jersey, USA). Resibufogenin and bufalin were provided by PhytoLab ® (Vestenbergsgreuth, Bavaria, Germany).

2.2. Animal material

The venom of *Rhinella marina (L.)* was purchased from Alpha-Biotoxine® (Montroeul-au-bois B-7911, Belgium). The venom was collected through manual compression of the specimens paratoid glands. The white liquid was collected onto a watch glass. Secretions were air-dried to obtain a crystal-like form.

2.3. Extraction process

The extraction step consists of sonication-assisted four-solvent process (in order: n-heptane, dichloromethane, ethyl acetate, methanol). The venom was grounded up finely and transferred into a borosilicate glass conical-bottom recipient and the first solvent (i.e., n-heptane) was added (ratio 1:20 m/v). The recipient was briefly vortexed and then placed in an ultrasonic bath (Branson® 3510, Danbury, CT, USA) for 60 min at room temperature. After being allowed to settle for 15 min approximately, the supernatant was filtered on a PTFE membrane (∅ = 0.45 µm, Whatman, Buckinghamshire, UK) and stored in a tared brown-glass vial. The venom pellet was placed under a gentle stream of nitrogen (Sample Concentrator EVAEC1-S, VLM, Bielefeld, Germany) until completely dry and the process was repeated with the following solvents. The four extracts were evaporated to dryness under nitrogen. Extraction yields (%, m/m) were evaluated by calculating the following ratio: (dry residue mass/ground-up venom mass)*100.

2.4. Fractionation process

2.4.1. Flash chromatography

The crude extracts underwent fractionation by flash chromatography. Pre-packed silica columns were used (12 g, $\varnothing_{particles}$ = 30 µm, Interchim, Montluçon, France). Samples were loaded using the dry-load technique. An aliquot of the liquid extract was mixed silica gel to a ratio of 1:4 (v/v) until a paste-like consistency was obtained. The mixture was transferred into an adapted dry-load cartridge. The eluants were A = ultrapure water and B = acetonitrile. Elution was performed using the gradient mode as follows: 100% B for 6.5 min, followed by linear decrease from 100% to 5% B over a period of 14 min and a final decrease from 5% to 0% B for the remaining 6 min. The fractionation run was followed by a rinsing step with water acidified with 0.1% TFA. The flow was set at 15 mL/min. The collection threshold was set for all peaks with an intensity greater than 5 mAU.

2.4.2. Preparative TLC

Fraction F2 that was obtained following the fractionation of the methanolic crude extract underwent a supplementary fractionation step. For this purpose, preparative thin-layer chromatography was performed. An aliquot of the liquid fraction sample was deposited manually on the silica plate (PLC silica gel 60 F254 2 mm, Merck, Darmstadt, Germany). The mobile phase was composed of the upper phase of a n-butanol/water/ethyl acetate (20/10/5) mixture. After visualization under UV at 254 nm, the zones of interest were scratched. The scraped silica was extracted with methanol by vortexing and ultrasonication for 60 min. After centrifugation, the supernatant was filtered on a PTFE membrane (∅ = 0.45 µm, Whatman, Buckinghamshire, UK) and stored in a tared brown-glass vial. Each sub-fractions were evaporated to dryness under nitrogen.

2.5. Chemical profile of extracts and fractions

For each sample, an aliquot was prepared at 1.0 mg/mL and 10 µL were injected for analysis. The analyses were performed on a Luna C18 (2) (250 × 4.6 mm, i.d., particle size: 5 µm, pore size: 100 Å) from Phenomenex®. The mobile phases were composed of A = ultrapure water with 0.5% acetic acid and B = acetonitrile. Gradient elution was performed as follows: isocratic at 8% B from 0 to 2 min, from 8% B to 55% B over 48 min, followed by an abrupt increase to 100% B in 1 min and stay at that for 10 min, and finally from 100% B to 8% B between 61 min and 63 min. The flow was set at 0.5 mL/min. The detection wavelength was set at 280 nm.

2.6. Antiplasmodial evaluation

2.6.1. Parasites and cultures

Plasmodium falciparum laboratory-adapted strains 3D7 and W2 were maintained in continuous culture following the protocol proposed by Trager and Jensen (Trager 1995) with some modifications. Parasites were cultured in complete medium supplemented at 5% hematocrit (A Rh^{+}). Briefly, complete medium was prepared from RPMI 1640 powder (25 mM Hepes, 2 mM L-Glutamine) supplemented with 25 mM $NaHCO_3$, 0.5% AlbuMax™ II, 2 mM Hypoxanthine and 0.002% Gentamicin. Cultures were incubated at 37 °C under humid atmosphere in a gas mixture containing 5% O_2, 5% CO_2, 90% N_2. Cultures were diluted with fresh RBCs every other day.

2.6.2. SYBR Green I fluorescence assay

Cultures were synchronized 96 h prior to plate seeding. The sorbitol method was used to achieve synchronicity. Briefly, whole cultures were incubated with a 5% sorbitol solution at 37 °C for 15 min and then submitted to successive centrifugation cycles before being finally put back in continuous culture as described previously. The infected RBC suspension was seeded in a 96-well plate with a parasitemia of 0.5% and

a hematocrit of 4%. Stock solutions were prepared in 100% DMSO at 10 mg/mL for all samples. Final tested concentrations ranged from 0.39 μg/mL to 100 μg/mL (two-fold dilution). Chloroquine was used as positive control for 3D7 and mefloquine for W2. A solution at 10% DMSO (diluted in culture medium) was prepared as negative control (1% DMSO in the wells, no toxicity was observed at this concentration). The background signal was considered by seeding some wells with uninfected RBCs suspension. Plates were treated and incubated at 37 °C under humid atmosphere in a gas mixture containing 5% O_2 for 72 h. Post-incubation, plates were placed at −20 °C for 12 h then thawed at room temperature. After homogenisation, 100 μL from each well were transferred in a black-bottomed plates containing 100 μL of SYBR Green I nucleic acid stain (Invitrogen®, Thermo Fisher Scientific, Waltham, MA, USA) diluted in the lysis buffer (0.2 μL of SYBR Green I/mL of lysis buffer [Tris (20 mM, pH = 7.5 adjusted with HCl 5 M), EDTA (5 mM), saponin (0,008%), triton X-100 (0,08%)]). Plates were incubated at room temperature in the dark for 1 h. Fluorescence was read out at λ_{ex} = 485 nm and λ_{em} = 530 nm.

2.7. Hemolytic activity

The hemolytic activity of the samples was evaluated according to Dos Santos et al. (Santos et al., 2010) with some modifications. Human RBCs were washed with ice-cold Phosphate Buffer Saline (PBS) by centrifugation at 3200×*g* for 5 min (repeated until clear supernatant is obtained). A RBCs suspension at 2% was prepared in PBS. The suspension was seeded in a 96-well plate. Samples were prepared in the same way as mentioned above. Triton X-100 1% in PBS (0.1% Triton X-100 in the wells) was prepared as the positive control. A solution at 10% DMSO in PBS was prepared as negative control (1% DMSO in the wells, no hemolytic activity was observed at this concentration). Plates were incubated at 37 °C for 1 h and then centrifuged at 1000×*g* for 5 min. 50 μL of supernatant was transferred from each well into a new plate and absorbance was read at 405 nm which displayed best dynamic range.

2.8. Cytotoxic evaluation

2.8.1. Cell lines and cultures

FHs74int cells (human fetal intestinal epithelial cells, ATCC # CCL-241, American Type Culture Collection, St. Cloud, MN, USA) were cultured in Hybri-Care medium (46-X, American Type Culture Collection, St. Cloud, MN, USA) supplemented with $NaHCO_3$ (1.5 g/L), FBS 10%, recombinant hEGF (30 ng/mL) and PenStrep 1% and maintained at 37 °C under humid atmosphere in a gas mixture containing 5% CO_2. HUVEC cells (human large vessel endothelial cells, PromoCell # C-12203, PromoCell, Heidelberg, Germany) were cultured in Medium 200 (Gibco®, Thermo Fisher Scientific, Waltham, MA, USA) supplemented with Low Serum Growth Supplement 2% and were also maintained at 37 °C under humid atmosphere in a gas mixture containing 5% CO_2.

2.8.2. MTT assay

FHs74Int cells and HUVEC cells were seeded in 96-well plates at 20,000 cells/well and 10,000 cells/well respectively and grown at 37 °C for 24 h before treatment. Stock solutions were the same as mentioned previously. Final tested concentrations ranged from 10^{-7} μg/mL to 10 μg/mL (ten-fold dilution). Digoxin was used as positive control for both cell lines with concentrations ranging from 10^{-8} μM–1 μM (ten-fold dilution). A solution at 1% DMSO (diluted in culture medium) was prepared as negative control (0.1% DMSO in the wells, no toxicity was observed at this concentration). After 72 h, the plates were rinsed with PBS and 200 μL of MTT [3(-(4,5-dimethylthiazol-2-yl)-2,5-diphenyltetrazolium bromide)] solution at 0.5 mg/mL (the solution was prepared in PBS when working with FHs74int cells and in the supplemented Medium 200 for HUVEC cells). The plates were incubated at 37 °C for a further 4 h after which the MTT reagent was replaced by 100 μL of DMSO. The absorbance was read at 570 nm.

2.8.3. Crystal violet assay

Cells were seeded in the same manner as described for the MTT assay. The tested concentrations and the negative control were also prepared identically. The positive control was also the same. After a 72 h treatment period, plates were rinsed with PBS and cells were fixed with 100 μL of 0.35% glutaraldehyde for 15 min. Plates were stained with 100 μL of a 0.05% crystal violet solution for 30 min after which the dye was discarded and the plates were extensively rinsed under a gentle stream of distilled water. 100 μL of Triton X-100 at 0.2% were added and the plates were gently and constantly agitated for 30 min. The absorbance was read at 570 nm.

2.9. Homology modeling of PfATP4

The sequence of *Plasmodium falciparum* cation ATPase (*PfATP4*) was retrieved from UniProt (Bateman et al., 2017) database (ID: Q9U445, 1, 264 residues). To select a template, we compared the *PfATP4* sequence with Protein Data Bank (PDB) sequences by means of local alignment with BlastP (Ramsay et al., 2000). We used a word size of 6 and the 10 most similar sequences were recorded. Two substitution matrices were considered (BLOSUM45 and BLOSUM62) and the Gap Opening Penalty and Gap Extension Penalty scores were set to 11 and 1, respectively. We compared the 10 templates obtained with the two sequence alignments, *i.e.,* with BLOSUM45 and BLOSUM62 substitution matrices and we selected only the templates for which the resolution of the crystal structure is below 3.0 Å. We found that two templates are retrieved in both sequence alignments: a Na^+,K^+-ATPase structure (PDB ID: 3WGU, chain A) and a Ca^{2+}-ATPase structure (PDB ID: 6ZHH, chain A). Both templates were considered to build homology models of *PfATP4* with MODELLER 10.1 (Sali et al., 2002). We performed a global multiple sequence alignment between *PfATP4* sequence and sequences extracted from the two selected templates (3WGU and 6ZHH structures). For this, the SALIGN procedure as implemented within MODELLER 10.1 was employed. Based on this alignment, we built 100 homology models using the spatial restraints approach of MODELLER 10.1 (AutoModel procedure). The best homology model, *i.e.,* with the most negative DOPE score (Shen and Sali 2006), was selected for further loop optimization. For this, loops were derived from the multiple sequences alignment and 20 models were generated. A statistical potential (DOPELoop Score) was used in combination with MM/GBSA implicit solvation to classify and to select the best models. Quality validation of the selected homology model was done with PROCHECK (Laskowski et al., 1993). The resulting Ramachandran plot showed that 95.1% residues are in allowed regions, giving a certain confidence on the quality of the *PfATP4* homology model to be used for subsequent docking calculations.

2.10. Molecular docking of resibufogenin with PfATP4

The resibufogenin ligand was built within the Avogadro molecular editor (Hanwell et al., 2014). Molecular mechanics calculations were then achieved within Avogadro to optimize the geometry of the ligand by means of a steepest descent optimization (10,000 steps) with the MMFF94 force field (Halgren 2000). The energy convergence criterion was set at 10^{-7} kJ mol^{-1} for the energy minimization procedure. We used the homology model of *PfATP4* described above as docking target. Blind docking calculations were carried out on the entire surface of the *PfATP4* to detect potential binding sites of resibufogenin. For this, we employed two docking software: the *QuickVina-W* 1.1 package (Hassan et al., 2017), optimized for wide search space and blind docking, and *PSOVina2 2.0*, another fork of AutoDock Vina based on Particle Swarm Optimization (PSO) algorithm to sample the surface of the target (Tai et al. 2018). For each docking algorithm, we performed 200 docking runs (400 in total for both methods) in a docking box of 100 × 84 × 126 Å with a spacing of 1.0 Å and a large exhaustiveness value of 256. For each docking run, we retained the best docking solution and the 400 docking solutions were then clustered, filtered and rejected if they are

not in the extracellular regions of *PfATP4*. Among the 400 docking solutions, we thus obtained a subset of 37 docking solutions (19 for QuickVina-W 1.1 and 18 for PSOVina2 2.0) located in two neighboring binding sites. To refine our docking solution, we then completed additional docking calculations centered on these two neighboring binding sites with the original AutoDock Vina package (Trott and Olson 2012), using then a smaller docking box of 30 × 30 × 30 Å (spacing of 1.0 Å) and still an exhaustiveness value of 256. We performed 20 runs with different seed numbers on each binding site, resulting at the end on a set of 40 docking solutions of the resibufogenin ligand on the *PfATP4* structure. For each docking calculation, the ligand was set as flexible entity whereas the target was considered as a rigid object. The PyMOL molecular visualization software was used for structural analysis as well as for depicting the binding modes (DeLano 2002).

2.11. Data analysis

Antiplasmodial activity was expressed using IC_{50} values whereas cytotoxicity on normal cells was expressed using LD_{50} values. IC_{50} and LD_{50} were calculated from dose-response curves using the GraphPad Prism 8 software (San Diego, CA, USA). When applicable, data are expressed as (mean ± standard deviation). For all biological assays, three biologic replicates (n = 3) were performed, each containing 3 technical replicates (n = 3). When applicable, values were compared with ANOVA tests and Tukey's multiple comparisons test. All were conducted with GraphPad Prism 8. For all analyses, $p < 0.05$ was considered statistically significant (*), p values inferior to 0.01 (**), 0.001 (***), 0.0001 (****) were considered highly significant.

3. Results & discussion

3.1. Antiplasmodial activity of crude extracts

The generated crude extracts were evaluated for their antiplasmodial activity and more precisely their activity on the asexual blood stage of *P. falciparum*. Only extracts displaying IC_{50}s < 100 µg/mL (Kwansa-Bentum et al., 2019) were further considered for fractionation. Fractions were evaluated in their turn for antiplasmodial effect. In some cases, it was possible de obtain sub-fractions that underwent the same process. All samples of interest had their cytotoxicity assessed on normal human cells and the selectivity index (SI) was calculated when applicable.

The characterization of each crude extract (see Supplementary data Fig. S1) was carried out by HPLC-UV/MS (Fig. 2A). The identification of compounds was performed partly by comparing molecular ion $[M+H]^+$ mass to charge ratios to published detailed LC-HRMS analyses (Jing et al., 2013; Cao et al., 2019; Schmeda-hirschmann, Quispe, and Vargas

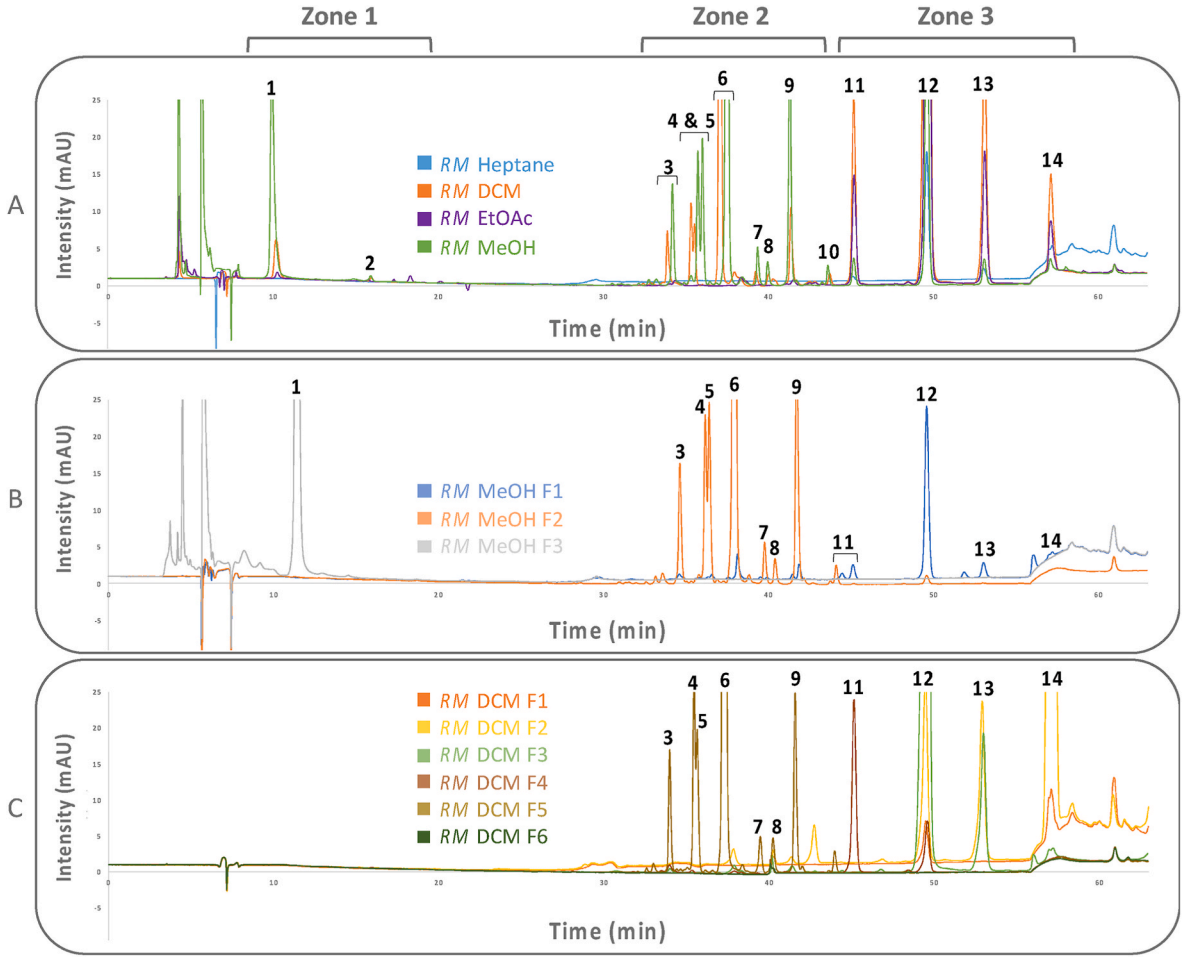

Fig. 2. LC-UV (λ = 280 nm) fingerprints of the four crude extracts of (**A**) *Rhinella marina* venom, (**B**) *RM* MeOH fractions (F1 – F3) and (**C**) *RM* DCM fractions (F1 – F6). The LC-UV system was also coupled to a MS detector (simple quadrupole, ESI voltage 3.5 kV, source temperature 200 °C, cone voltage 20 V, m/z range: 100–1000) which allowed preliminary peak identification. Proposed compound identification is as follows – 1: Dehydrobufotenine $[M+H]^+ = 203.0$ *m/z*; 2: Suberoyl arginine $[M+H]^+ = 330.9$ *m/z*; 3: Bufalin-3-pimeloyl arginine ester $[M+H]^+ = 685.2$ *m/z*; 4: 3-(N-succinyl argininyl) cinobufagin $[M+H]^+ = 699.5$ *m/z*; 5: Telocinobufotoxin $[M+H]^+ = 715.2$ *m/z*; 6: Marinobufotoxin $[M+H]^+ = 713.2$ *m/z*; 7: Unknown (*685.1 m/z*); 8: 3-(N-adipoyl argininyl)-Scillarenin $[M+H]^+ = 669.1$ *m/z*; 9: Bufalitoxin $[M+H]^+ = 699.2$ *m/z*; 10: Resibofotoxin $[M+H]^+ = 697.0$ *m/z*; 11: Telocinobufagin $[M+H]^+ = 403.0$ *m/z*, $[M + \mathbf{CH_3CN} + H]^+ = 444.0$ *m/z*; 12: Marinobufagenin $[M+H]^+ = 401.3$ *m/z*, $[M + \mathbf{CH_3CN} + H]^+ = 442.0$ *m/z*, $[2M + H]^+ = 801.0$ *m/z*; 13: Bufalin $[M+H]^+ = 387.0$ *m/z*, $[M + \mathbf{CH_3CN} + H]^+ = 428.0$ *m/z*; 14: Resibufogenin $[M+H]^+ = 385.0$ *m/z*, $[M + \mathbf{CH_3CN} + H]^+ = 426.0$ *m/z*.

2016) of several *RM* toad secretions and by complementary confirmation by NMR and QTOF analysis. Also, reference standards of four bufagins (telocinobufagin, marinobufagenin, bufalin and resibufogenin) were used to help identify compounds. The developed LC method allowed to separate the extracts' components into three distinct fingerprint regions. Based on previously reported data, we could suggest that zone 1 contained more polar compounds among which alkaloids and arginine derivates resulting most likely from the hydrolysis of bufotoxins in C_3. Zone 2 followed and most likely contained bufotoxin-type compounds. Lastly, previous data and the use of reference compounds suggested that zone 3 contained mainly bufagin-type compounds. The *n*-heptane crude extract was rather poor compared to dichloromethane, ethyl acetate and methanol ones. This was to be expected as heptane is more commonly used for lipid extraction and toad venoms are not known to contain high amounts of lipidic derivatives, if any. However, marinobufagenin (MBG) was identified but only in a small proportion. The dichloromethane (DCM) extract was richer and contained both bufotoxins and bufagins. The latter were present in higher proportions. Bufagins family display more apolar characteristics than bufotoxins. This is due to the fact that bufagins lack of a polar moiety in position C_3. Ethyl acetate (EtOAc) offered a more selective extraction as in it contained bufagins exclusively with MBG being the main component. The methanol (MeOH) extract, much like DCM, extracted bufagins and bufotoxins. However, due to the more polar nature of MeOH, bufotoxins were found in higher proportions than bufagins. Following antiplasmodial evaluation, only the DCM and MeOH extracts exhibited interesting activities on both sensitive and resistant strains (Table 1). No further analyses were conducted on the heptane and EtOAc extracts (IC_{50}s > 100 μg/mL).

To better understand the selection of our samples, Fig. 3 depicts the overall extraction, fractionation and sub-fractionation processes. The light green boxes represent samples that displayed IC_{50}s < 100 μg/mL when tested *in vitro* on the parasites and were considered for further testing and analysis. The grey boxes are the extracts and samples that didn't display interesting antiplasmodial activity and that were not retained.

3.2. Fractionation and antiplasmodial evaluation

The methanolic (*RM* MeOH) and dichloromethane (*RM* DCM) crude extracts were fractionated by flash chromatography (Fig. 4).

Three fractions resulted from *RM* MeOH crude extract and were characterized by LC-UV/MS (F1 – F3) (Fig. 3B). *RM* MeOH F1 (yield: 2%, m/m) was found to contain mainly bufagins whereas RM MeOH F2 (yield: 43%, m/m) contained mostly bufotoxins. A third fraction (yield: 23%, m/m) was obtained after rinsing the silica cartridge with a strong eluant (acidified water 0.1% TFA). *RM* MeOH F3 contained highly polar components of the venom such as dehydrobufotenin, an alkaloid, suberoyl arginine and 19-oxo-cinobufagin, a polar bufagin. The same process was applied to *RM* DCM crude extract and this gave way to six fractions (F1 – F6) that were also characterized (Fig. 3C). *RM* DCM F1 (yield: 5%, m/m) led to a bright yellow residue but its content remained unidentified following MS analysis. The main components of RM *DCM* F2 (yield: 3%, m/m), F3 (yield: 64%, m/m) and F4 (yield: 8%, m/m) were resibufogenin, marinobufagenin and telocinobufagin respectively. The bufotoxin fraction of the extract was identified as *RM* DCM F5 (yield: 13%, m/m). The sixth fraction was also obtained post-rinsing but its content could not be identified. Flash chromatography allowed to fractionate the crude extracts by class of compounds and in some cases isolated compounds with relatively high percentages of purity. The fractions were tested *in vitro* to evaluate their antiplasmodial potential, following the same protocol as for the crude extracts. Among these, three fractions were highlighted as displaying an interesting effect: *RM* MeOH F1, *RM* MeOH F2 and *RM* DCM F2 (Table 1). *RM* MeOH F2 displayed the least promising activity but was the only fraction with a yield high enough to allow an extra round of fractionation this time using preparative TLC. Four sub-fractions (Fig. S2) were generated (F2.1 – F2.4) among which F2.1 was the most active. *RM* MeOH F1 demonstrated an activity worthwhile investigating with parasite viability levels dropping below 30–40% for both strains. It was composed of the

Table 1
Biological evaluations of crude extracts, fractions and reference compounds.

	Samples	Antiplasmodial activity[a]		Cytotoxicity[b]			
		SYBR Green I assay		MTT assay		CVS assay	
		*Pf*3D7	*Pf*W2	FHs74Int	HUVEC	FHs74Int	HUVEC
RM crude extracts	DCM	48 ± 6	53.0 ±± 0.1	0.086 ±± 0.002	0.0158 ±± 0.0004	0.0490 ±± 0.0001	0.036 ±± 0.005
	MeOH	16 ±± 3	18 ±± 5	0.1867 ±± 0.0006	0.0363 ±± 0.0005	0.57 ±± 0.02	0.085 ±± 0.003
RM DCM fractions	F 2	46 ±± 5	39 ±± 2	n.t.[c]	n.t.[c]	n.t.[c]	n.t.[c]
RM MeOH fractions	F 1	44 ±± 4	42 ±± 6	0.145 ±± 0.003	0.0148 ±± 0.0005	0.128 ±± 0.002	0.036 ±± 0.006
	F 2	59 ±± 1	60 ± 10	0.239 ±± 0.001	0.09 ±± 0.01	0.2500 ±± 0.0004	0.0819 ±± 0.0010
RM MeOH F2 sub-fractions	F 2.1	47 ±± 1	>100	48.9 ±± 0.4	46 ±± 4	>100	75 ±± 1
	F 2.2	60 ±± 8	>100	2.57 ±± 0.04	0.16 ±± 0.01	2.0000 ±± 0.0004	0.37 ±± 0.01
	F 2.4	52 ±± 5	>100	0.41 ±± 0.03	0.013 ±± 0.002	0.48 ±± 0.04	0.030 ±± 0.004
Commercial standards	MBG	92 ±± 1	>100	1.29 ±± 0.05	2.2 ±± 0.1	1.8 ±± 0.1	0.77 ±± 0.02
	RBG	29 ±± 8	23 ±± 1	0.191 ±± 0.002	0.034 ±± 0.002	0.695 ±± 0.010	0.047 ±± 0.002
	BFL	>100	96 ± 9	0.0038 ± 0.0002	0.00074 ± 0.00005	0.03439 ± 0.00006	0.00095 ± 0.00004
Positive controls	CQ	0.0183 ± 0.0007 ((57 ± 2) nM)[d]	n.t.	**	**	**	**
	MQ	n.t.	0.010 ± 0.002 ((26 ± 5) nM)[d]	**	**	**	**
	Digoxin	n.t.	n.t.	0.031 ± 0.004 ((0.040 ± 0.005) μM)	0.04 ± 0.01 ((0.05 ± 0.02) μM)	0.013 ± 0.002 ((0.016 ± 0.003) μM)	0.013 ± 0.001 ((0.017 ± 0.001) μM)

n.t. not tested.
**Tested compounds did not display any toxicity on normal human cells for the effective concentration range (0.78–200 nM).
The full table with all the tested extracts and fractions can be found in the **Supplementary data** (Table S5).
[a] IC_{50} values (μg/mL) presented as the mean ±± standard deviation of three experiments performed in triplicates, treatment for a period of 72 h.
[b] LD_{50} values (μg/mL) presented as the mean ±± standard deviation of three experiments performed in triplicates, treatment for a period of 72 h.
[c] The cytotoxicity of *RM* DCM F2 could not be assessed because the quantity following fractionation was not sufficient.
[d] These IC_{50} values were compared to the ones evaluated using the Gold-standard optical microscopy approach (protocol adapted from Rieckmann et al., (1978)). The same concentration ranges as for the SYBR Green I assay were tested (0.78–200 nM) for a treatment period of 72 h. For each compound (CQ and MQ), three experiments were performed in triplicates. Upon comparison of the IC50 values, no statically significant difference was highlighted. Furthermore, both assays gave way to similar profiles of viability curves (data not shown).

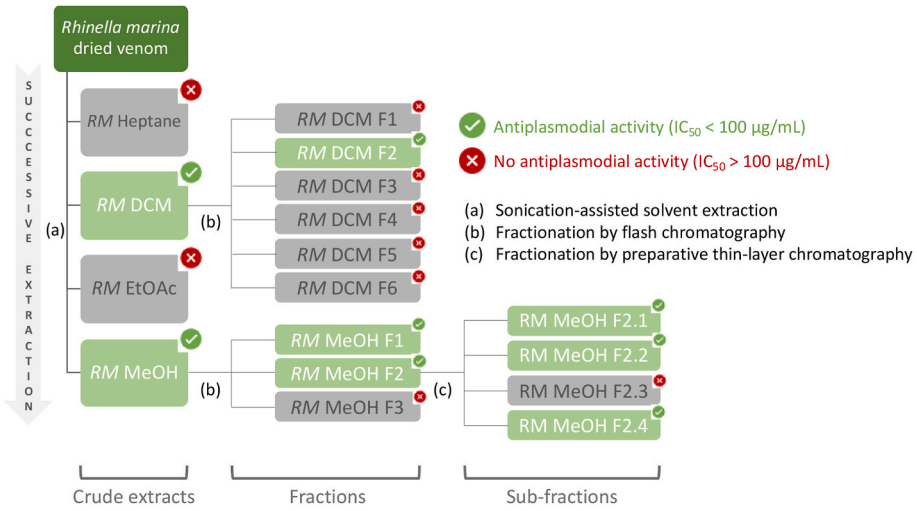

Fig. 3. Extraction and fractionation scheme of samples displaying antiplasmodial activity.

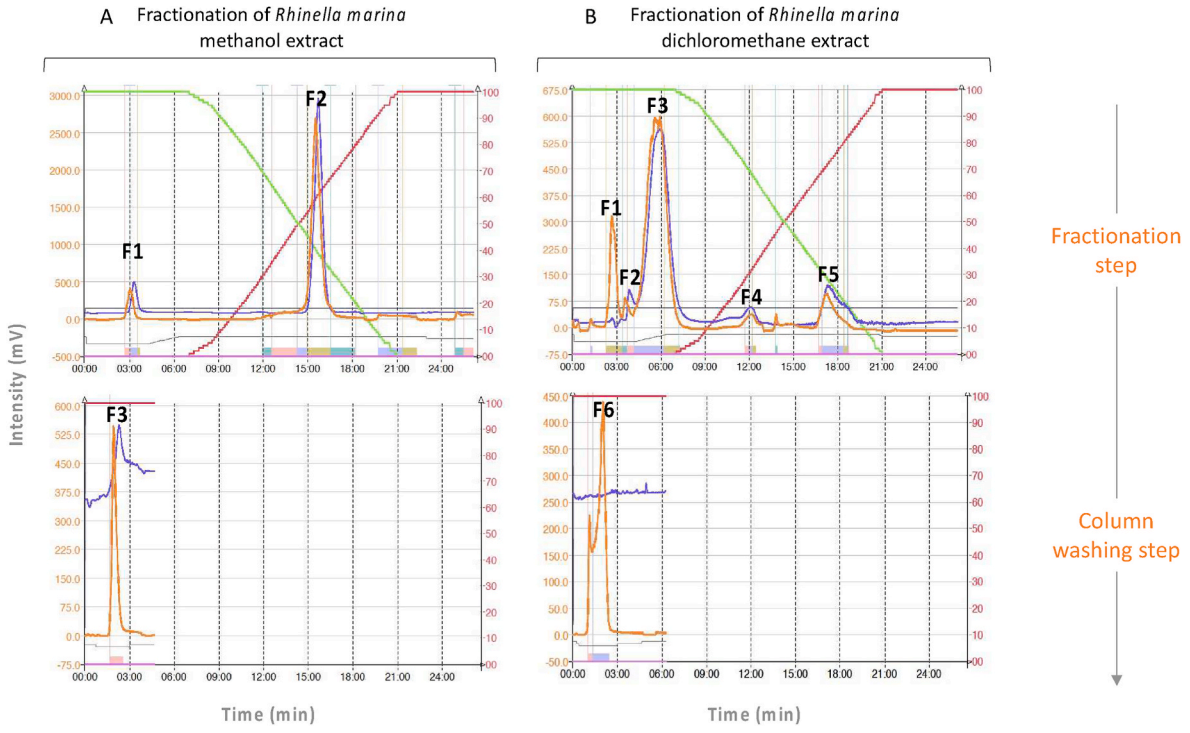

Fig. 4. Flash chromatograms following the fractionation of *RM* MeOH (A) and *RM* DCM (B) crude extracts (– UV detection channel at 296 nm; – ELSD detection channel). The eluant used for the initial fractionation step is composed of an acetonitrile:water gradient. The column is washed with water acidified by 0.1% TFA.

following: marinobufagenin (56.9%), bufalin (BFL) (5.2%), telocinobufagin (TBG) (4.2%), resibufogenin (RBG) (3%). *RM* DCM F2 also retained our attention since parasite viability dropped below 20% at the highest concentration after 72 h of treatment in both *Pf* strains. After further analysis, this fraction was found to contain resibufogenin (RBG) (74.2%), marinobufagenin (MBG) (10.8%) and bufalin (BFL) (9.8%). This particularly interesting fraction was analyzed by ^{1}H-NMR that confirmed RBG as being the major component (Fig. S3, Table S1). Among the retained fractions following flash chromatography, *RM* MeOH F1 and *RM* DCM F2 were the most promising ones. The main components were bufagins: TBG, MBG, BFL and RBG. The effect on parasite viability of these compounds was evaluated individually. Commercial standards were used to prepare the test solutions. RBG came out as the most active compound with IC_{50} values of (29 ± 8) µg/mL and (23 ± 1) µg/mL for 3D7 and W2 respectively. MBG exerted only a weak activity *in vitro* on the 3D7 strain. Whereas both BFL and TBG were excluded for not displaying interesting enough activities (Table 1). Interestingly, although these compounds possess similar structures, the effects observed varied greatly. Upon preliminary comparison of their structures, we could hypothesize that the most effective structure configuration for this class of compounds in terms of antiplasmodial activity was an epoxy-group in C_{14} – C_{15} and the lack of a hydroxyl-group in C_5 (Fig. 1).

When comparing the IC50s obtained on both strains for *RM* DCM, *RM* MeOH, *RM* DCM F2, *RM* MeOH F1, *RM* MeOH F2 and RBG, no statistically significant differences were highlighted. Keeping in mind that 3D7 is chloroquine-sensitive and W2 is chloroquine-resistant, some preliminary hypotheses could be drawn up regarding some potential

mechanism of action pathways. Similar IC_{50} values could suggest that the target is common in both strains. Studies have shown that the W2 strain has higher expression levels of the *Pfcrt* gene (Bray et al., 2005). This gene encodes for a transporter localized in the digestive vacuole of the parasite that is implicated in the resistance mechanisms against many antimalarials (especially chloroquine) (Shafik et al., 2020). Resistance is achieved by expulsing the drug from the digestive vacuole so that it cannot act on its target. Chloroquine inhibits the detoxification pathway of heme into hemozoin, but it can only do so by entering the digestive vacuole and staying there. Considering that similar responses were obtained in both strains for these samples, it could suggest that they do not act by inhibiting the hemozoin polymerization and that their target could lie outside the digestive vacuole of the parasite. At this stage however, the heme detoxification pathway cannot yet be set aside as a potential target. If our samples are shown not to be substrates of *Pfcrt*, they could still penetrate the digestive vacuole and target the formation of hemozoin. Lastly, RBG contains an epoxy moiety. We could also suggest that the epoxy ring could open in the presence of free heme (Fe (II)) and lead to the production of oxidative species which could impact the parasite's viability much in the same way as artemisinin derivates.

For *RM* MeOH F2.1, F2.2 and F2.4, only the 3D7 strain responded to the treatment. No antiplasmodial effects were observed in W2. In this case, the results suggest that the samples could exert their antiplasmodial properties through the same pathway as does chloroquine.

This constitutes a preliminary analysis and further studies are required to better understand the mechanisms at play.

3.3. Toxicity evaluation

As the purpose of this work is to identify new potential therapeutic candidates for human use, their toxicity on normal human cells was a primordial parameter to investigate. The hemolytic activity of all samples of interest was also evaluated. This latter aspect is a crucial character to consider especially since the pathogen's host cells are RBCs. Following our tests, none of the aforementioned samples displayed a hemolytic activity (Fig. S4). The hemolysis rates were comparable to those observed for known antimalarial drugs and it was shown that our samples did not exhibit hemolysis rates higher than the control compounds (i.e., chloroquine and dehydroartemisinin, data not shown). The toxicity on normal human cells was also assessed *in vitro* using two cell lines: FHs74int and HUVEC. Two complementary bioassays, MTT and Crystal Violet Stain (CVS), were used in parallel with the aim of better understanding the potential involved mechanisms of toxicity. The ideal candidate should display a high LD_{50} on normal cells and a low IC_{50} on the parasites giving us Selectivity Index ratio (LD_{50}/IC_{50}) values above 10. None of the samples tested met these requirements (see Supplementary data Table S4). This did not come to a surprise considering that bufadienolides are known for their toxicity and more so their cardiotoxicity. We did obtain an SI above 3 for one of the samples. This fraction, *RM* MeOH F2.1, contained polar compounds, suberoyl arginine and dehydrobufotenine as shown by NMR and MS (Fig. S5, Table S2). *RM* MeOH F2.1 was found to be active against 3D7 only and even so, viability merely dropped between 40 and 50% at the highest concentration. Therefore, among the highlighted compounds, resibufogenin and its antiplasmodial activity remain the most promising. Even if its selectivity index ratio is low, RBG could provide the basis for a novel antimalarial drug-scaffold. The long-term perspective would be to reduce the toxicity rate without compromising the therapeutic effect. With this perspective in mind, a preliminary investigation of the potential toxicity mechanisms was performed. Following statistical analyses (Table S3), LD_{50}s obtained for HUVEC cells were overall significantly lower than for FHs74int cells. The relative expression of the four isoforms of the Na^+/K^+-ATPase alpha-subunit was determined through qPCR. It showed that HUVEC cells had a higher content of 3 of these isoforms (Fig. S6). Linking the lower LD_{50} values and the higher levels of expression in HUVEC cells confirms that the tested samples exert one of their toxic effects on normal cells through inhibition of the NKA. MTT and CVS assays were considered because they allow to highlight different toxicity aspects. The MTT assay will highlight compounds that affect mitochondrial metabolism whereas CVS assay permits to quantify the percentage of cells still adhering meaning this test will allow to monitor if a substance affects cell adherence capacity, shape and morphology. Shifts in viability curves between the two tests for a same sample could have pointed to one toxicity mechanism in particular. However, no significant differences were observed when comparing the viability curves obtained with the MTT assay and the CVS assay for a same cell line and a same sample.

3.4. Molecular modeling

As mentioned earlier, the main target of bufadienolides, among which resibufogenin, is the NKA pump, an ATP-dependent transmembrane pump responsible for maintaining low intracellular Na^+ levels. *Plasmodium falciparum* also possesses a series of ATPase pumps. More recently, *PfATP4* has been considered has a potential new target for novel antimalarial drugs (Spillman and Kirk, 2015; Spillman et al., 2013; Dangi et al., 2019). Owing to its ability to block NKA's function, we investigated whether resibufogenin could potentially bind to *PfATP4,* as a possible mode of action regarding its antiplasmodial properties. For this purpose, an *in silico* approach was considered, using molecular docking calculations to study the possible binding mode of resibufogenin to *PfATP4*. To this aim, we first built a three-dimensional structure of *PfATP4* by using homology modeling methods (see Methods for computational details). We then obtained a set of 40 docking solutions in the extracellular region of *PfATP4* (see Methods). Most of the docking solutions, *i.e.,* 38 out of the 40, converge to the same binding mode with a docking score related to a binding energy of −8.6 kcal/mol. This affinity score is similar and slightly higher (in absolute value) than the −8.3 kcal/mol score suggested by Dangi et al. with indole-based chiral ligands on *PfATP4* (Dangi et al., 2019). Resibufogenin is docked in a transversal way to the axis formed by the transmembrane α-helices of *PfATP4* (Fig. 5A and Fig. S7).

A set of 12 *PfATP4* residues were detected near the resibufogenin (<5 Å), *i.e.,* six polar/charged residues (E125, N126, R1063, D1067, R1165, T1166), four hydrophobic/non-polar residues (I124, I1064, I1170, M1167), and two aromatic residues (Y1060, W1174). The resibufogenin is interacting through hydrogen bond (2.6 Å) between one oxygen atom of the lactone moiety and the hydrogen atom belonging to the amine fragment of the W1174 indole group (Fig. 5B). The same lactone moiety is also close (4.0 Å) to the guanidinium group of R1165 (Fig. 5B). The lactone of resibufogenin is thus stabilized by both polar contacts (R1165) and hydrogen bond (W1174). On the other part of the resibufogenin, the cyclohexanol moiety is involved in a hydrogen bond (Fig. 5C). We noted a 3.0 Å distance between the hydrogen atom of the hydroxyl group and the oxygen atom of the amide bond formed by residues E125 and N126, pointing out an important interaction between the resibufogenin and the backbone of *PfATP4* with two charged residues located on the surface of the receptor. In the central region of the ligand, the sterol fragment is quite exposed, although hydrophobic residues were observed in the neighborhood, for instance between the methyl group of resibufogenin 5-ring group and the sidechain of I1170.

A second binding mode was noticed among the 40 best docking solutions (Fig. 6A). This alternative binding mode was recorded only twice but with an important docking score of −8.5 kcal/mol, close to the score of the first binding mode (−8.6 kcal/mol). In this case, the resibufogenin ligand is oriented parallel to the axis formed by the bundle of α-helices of the *PfATP4* transmembrane domain, a rather different orientation that allows the resibufogenin to be more deeply bounded within the core of *PfATP4* (see Fig. S7 for the superimposition of both binding modes). In this binding mode, we detected more residues close (<5 Å) to the resibufogenin, (*i.e.,* 15 *PfATP4* residues instead of 12). Moreover, most of them are now hydrophobic/non-polar residues (I124, L127, V394, I397,

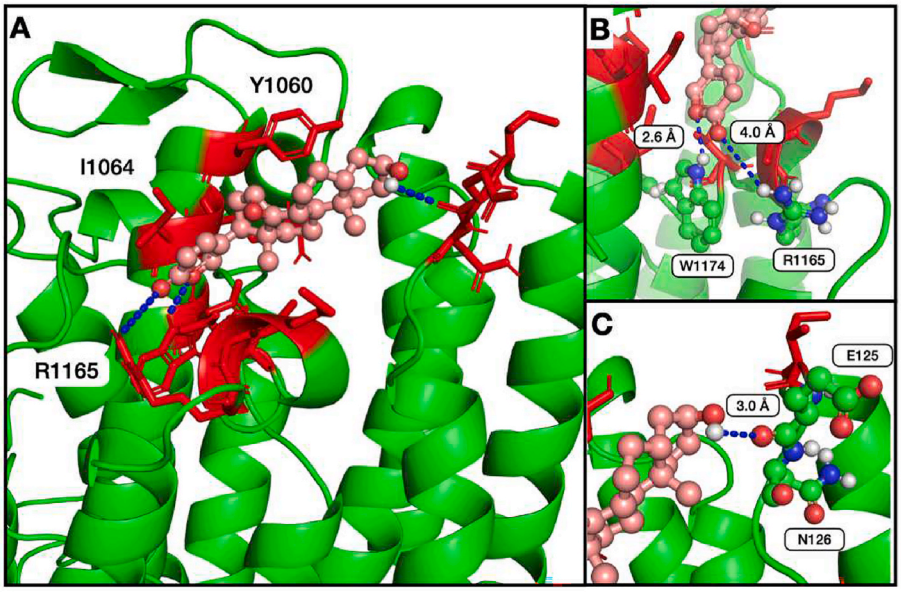

Fig. 5. A. Binding mode of the resibufogenin with *PfATP4*. The ligand resibufogenin is depicted in ball-and-stick representation (light pink), the *PfATP4* structure is represented in cartoon mode (green). The residues that are close to the ligand (<5 Å) are depicted in red using a stick representation. Principal interactions are depicted with blue dashed lines. **B.** Hydrogen bonds and polar contacts between the lactone moiety of the resibufogenin and the residues W1174 and R1165. **C.** Hydrogen bond between the cyclohexanol moiety of the resibufogenin and the backbone of the residues E125 and N126. (For interpretation of the references to colour in this figure legend, the reader is referred to the Web version of this article.)

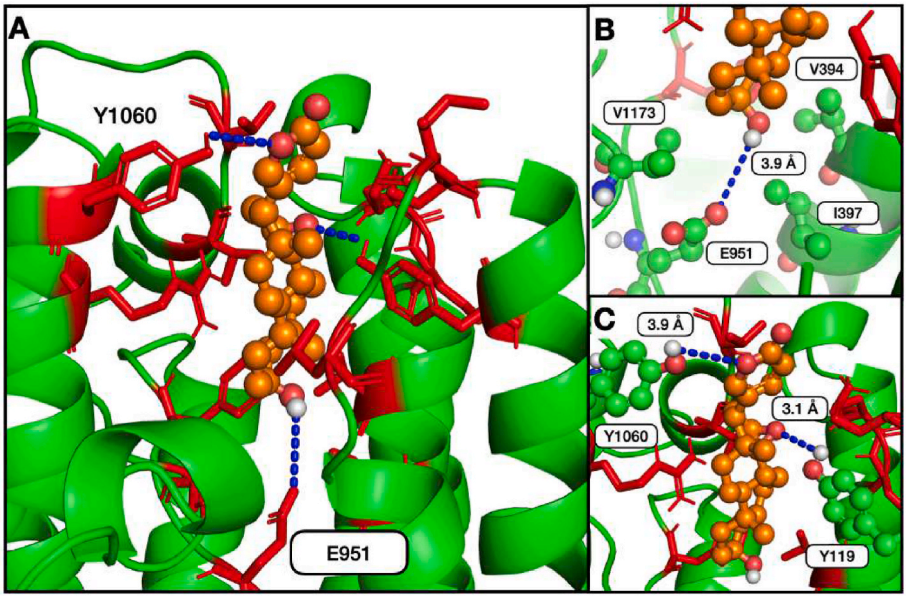

Fig. 6. A. Alternative binding mode of the resibufogenin to *PfATP4*. The ligand resibufogenin is depicted in ball-and-stick representation (orange), the *PfATP4* structure is represented in cartoon mode (green). The residues that are close to the ligand (<5 Å) are depicted in red with a ball-and-stick representation. Principal interactions are depicted with blue dashed lines. **B.** Hydrogen bonds and polar contacts between the cyclohexanol moietie of the resibufogenin and the residue E951. **C.** Hydrogen bonds between the lactone moiety and Y1060, and between the epoxide moiety of the resibufogenin and the residue Y119. (For interpretation of the references to colour in this figure legend, the reader is referred to the Web version of this article.)

V1042, V1044, V1173), whereas only four residues are polar/charged (S123, K389, D390, R1063), four are aromatic residues (Y119, F948, Y1060, E951).

There are thus only three residues (I124, R1063 and Y1060) that are similar for the two binding modes of resibufogenin to *PfATP4*, which shows that these two binding modes are quite different despite very similar docking scores. In the so-called second mode, the ligand is oriented in an opposite way to the first binding mode according to the orientation of lactone/cyclohexanol fragments with the axis formed by the α-helices of the transmembrane domain (see Fig. S7). The lactone moiety is now pointing through the extracellular part (apex) of the receptor, whereas it was close to the buried residue W1174 (with H-bond interaction) for the first binding mode. In terms of interaction, we thus observed that the hydroxyl group of the cyclohexanol moiety of resibufogenin is forming a hydrogen bond with one oxygen atom of the E951 side chain (3.9 Å), along with three hydrophobic residues (V394, I397, V1173) that formed a hydrophobic pocket around the cyclohexanol group of the ligand (Fig. 6B). Similarly, the hydrophobic residue L127 is also near the sterol moiety. On the other part of the ligand, we noted a hydrogen bond between the oxygen atom of the epoxide moiety and the hydrogen atom of the hydroxyl of Y119 (3.1 Å) as depicted in Fig. 6C. The internal-ring oxygen atom of the lactone moiety is also located at 3.9 Å to the hydrogen atom belonging to the hydroxyl moiety of Y1060. In contrast to the previous binding mode, the external-ring oxygen atom of the lactone is not interacting with close residues and is pointing towards the solution.

Interestingly, this second binding mode has some similarities with the binding mode between the Na^+,K^+-ATPase and bufalin, also a cardiotonic steroid ligand that differs with the resibufogenin only by the ring opening of the epoxy fragment. The superimposition of the extracellular domains of Na^+,K^+-ATPase, bound to bufalin, with our homology model of *PfATP4*, bound to resibufogenin, shows that both ligands are deeply docked in the same region and oriented in a similar way, i.e. in parallel to the bundle of the transmembranar α-helices (see Fig. S8).

The bufalin is even more deeply docked within the Na^+,K^+-ATPase core. We also observed that hydroxyl atoms of both cyclohexanol moieties are overlapping well, which tend to rationalize this alternative binding mode proposed by the docking calculations.

Following this preliminary molecular modeling investigation, it was revealed that the main chemical functions potentially involved were the hydroxyl-group in C_3, the δ-lactone ring in C_{17} and the steroid skeleton (see Fig. 1). The epoxy moiety was also shown to be potentially implicated in the binding process but in a lesser manner. Among these, the hydroxyl function in C_3 has already been reported as being crucial to the bioactivity of bufadienolides as well as the δ-lactone ring (Oliveira et al., 2021; Zhong et al., 2020; Shao et al., 2022).

As for the highlighted binding modes, further research into the structure of *PfATP4* would allow to identify its active sites which would lead to a better understanding of the binding interactions occurring in these regions (Rosling et al., 2018; Turner 2016). The efficacy of our samples could be tested *in vitro* and compared using wild-type *Pf* strains and strains resistant to known *PfATP4* inhibitors (Spillman et al., 2013). Another option will be to assess the effect of our samples on the ATPase activity of isolated parasite plasma membranes (Rosling et al., 2018).

4. Conclusion

In conclusion, our systematic approach was suitable for the fractionation of toad venom extracts and revealed that the venom of *Rhinella marina (L.)* could represent an interesting novel source of antiplasmodial compounds. The four-solvent extraction step constituted a good way to declutter the extracts thus rendering fractionation easier. Furthermore, the choice of solvents allowed to focus exclusively on small non-peptidic molecules. Flash chromatography had already been used, although rarely, to isolate pure compounds from toad venom extracts. In the context of this work, it was used not to purify but rather to generate crude fractions containing several compounds. Flash chromatography revealed itself to be a simple and rapid way to fractionate our crude extracts. Additionally, this technique was adapted to working with small amounts of samples which is not always the case for more frequently described fractionation methods such as open-column chromatography and preparative HPLC. Active fractions were shown to contain several bufadienolides, among which resibufogenin (RBG) displayed the most promising activity. To the best of our knowledge, this is the first time that RBG was shown to possess antiplasmodial properties. Although no hemolytic activity was observed, the selectivity for *Plasmodium falciparum* remains weak as RBG displays high toxicity against normal human cells. Regarding a potential mechanism of action, based on the *in-silico* approach, *PfATP4* can be considered to be a likely target and relevant binding modes were identified with high docking scores. All the results suggest that RBG could provide a promising scaffold basis for future antimalarial drugs. Undoubtedly, further studies are required, including chemical modifications of the RGB structure, to better understand the mechanisms of toxicity and the mode of action of this potential antimalarial drug.

Acknowledgment

The authors warmly acknowledge Prof. Pierre Duez and his team for their expertise and kindly sharing their equipment. The authors also wish to thank Prof. Pascal Gerbaux and Irène Semay for their help during MS analysis, Dr Céline Hénoumont for her assistance for generating NMR data and Prof. Carmen Burtea for giving us access to her laboratory's equipment. The University of Mons is also acknowledged for the funding a full PhD grant for Mathilde Wells. M.F. and M.S. thank FNRS-FWO Excellence of Science project PRECISION (Grant No 30650939). Computational resources have been provided by the Consortium des Équipements de Calcul Intensif (CÉCI), funded by FNRS (Grant No. 2.5020.11) and by the Wallonia Region.

Appendix A. Supplementary data

Supplementary data to this article can be found online at https://doi.org/10.1016/j.ijpddr.2022.10.001.

References

Arya, Aditi, Kojom Foko, Loick P., Chaudhry, Shewta, Sharma, Amit, Singh, Vineeta, 2021. Artemisinin-based combination Therapy (ACT) and drug resistance molecular markers: a systematic review of clinical studies from two malaria endemic regions - India and sub-Saharan Africa. Int. J. Parasitol.: Drugs Drug Resist. 15, 43–56. https://doi.org/10.1016/j.ijpddr.2020.11.006. November 2020.

Atanasov, Atanas G., Zotchev, Sergey B., Dirsch, Verena M., Orhan, Ilkay Erdogan, Banach, Maciej, Rollinger, Judith M., Barreca, Davide, et al., 2021. Natural products in drug discovery: advances and opportunities. Nat. Rev. Drug Discov. 20 (3), 200–216. https://doi.org/10.1038/s41573-020-00114-z.

Bagrov, Alexei Y., Shapiro, Joseph I., Fedorova, Olga V., 2009. Endogenous cardiotonic steroids: physiology, pharmacology, and novel therapeutic targets. Pharmacol. Rev. 61 (1), 9–38. https://doi.org/10.1124/pr.108.000711.

Banfi, Finger, Felipe, de Sena Guedes, Karla, Andrighetti, Carla Regina, Aguiar, Ana Carolina, Debiasi, Bryan Wender, Noronha, Janaina da Costa, Rodrigues, Domingos de Jesus, Vieira Júnior, Gerardo Magela, Marinho Sanchez, Bruno Antonio, 2016. Antiplasmodial and cytotoxic activities of toad venoms from Southern Amazon, Brazil. Kor. J. Parasitol. 54 (4), 415–421. https://doi.org/10.3347/kjp.2016.54.4.415.

Bateman, Alex, Martin, Maria Jesus, O'Donovan, Claire, Magrane, Michele, Alpi, Emanuele, Antunes, Ricardo, Bely, Benoit, et al., 2017. UniProt: the universal protein knowledgebase. Nucleic Acids Res. 45 (D1), D158–D169. https://doi.org/10.1093/nar/gkw1099.

Bedane, Kibrom Gebreheiwot, Brieger, Lukas, Strohmann, Carsten, Seo, Ean Jeong, Efferth, Thomas, Michael Spiteller, 2020. Cytotoxic bufadienolides from the leaves of a medicinal plant melianthus comosus collected in South Africa. Bioorg. Chem. 102 (February), 104102 https://doi.org/10.1016/j.bioorg.2020.104102.

Boussaroque, Agathe, Fall, Bécaye, Madamet, Marylin, Camara, Cheikhou, Benoit, Nicolas, Fall, Mansour, Nakoulima, Aminata, et al., 2016. Emergence of mutations in the K13 propeller gene of Plasmodium falciparum isolates from Dakar, Senegal, in 2013-2014. Antimicrob. Agents Chemother. 60 (1), 624–627. https://doi.org/10.1128/AAC.01346-15.

Bray, Patrick G., Martin, Rowena E., Tilley, Leann, Ward, Stephen A., Kirk, Kiaran, Fidock, David A., 2005. Defining the role of PfCRT in Plasmodium falciparum chloroquine resistance. Mol. Microbiol. 56 (2), 323–333. https://doi.org/10.1111/j.1365-2958.2005.04556.x.

Cao, Yueting, Wu, Jiheng, Pan, Hongye, Wang, Longhu, 2019. Chemical profile and multicomponent quantitative analysis for the quality evaluation of toad venom from different origins. Molecules 24 (19). https://doi.org/10.3390/molecules24193595.

Chen, Hu, Meng, Yu Hui, Guo, De An, Liu, Xuan, Liu, Jun Hua, Hu, Li Hong, 2015. New cytotoxic 19-Norbufadienolide and Bufogargarizin isolated from chan su. Fitoterapia 104, 1–6. https://doi.org/10.1016/j.fitote.2015.05.011.

Dagan, Arie, Leah Efron, Gaidukov, Leonid, Mor, Amram, Ginsburg, Hagai, 2002. In vitro antiplasmodium effects of dermaseptin S4 derivatives. Antimicrob. Agents Chemother. 46 (4), 1059–1066. https://doi.org/10.1128/AAC.46.4.1059-1066.2002.

Dangi, Poonam, Jain, Ravi, Mamidala, Rajanikanth, Sharma, Vijeta, Agarwal, Shalini, Bathula, Chandramohan, Thirumalachary, M., Sen, Subhabrata, Singh, Shailja, 2019. Natural product inspired novel indole based chiral scaffold kills human malaria parasites via ionic imbalance mediated cell death. Sci. Rep. 9 (1), 1–17. https://doi.org/10.1038/s41598-019-54339-z.

DeLano, Warren L., 2002. Unraveling hot spots in binding interfaces: progress and challenges. Curr. Opin. Struct. Biol. 12 (1), 14–20. https://doi.org/10.1016/S0959-440X(02)00283-X.

Dick, Claudia F., Meyer-Fernandes, José Roberto, Vieyra, Adalberto, 2020. The functioning of Na+-ATPases from Protozoan parasites: are these pumps targets for antiparasitic drugs? Cells 9 (10), 1–12. https://doi.org/10.3390/cells9102225.

Flannery, Erika L., McNamara, Case W., Kim, Sang Wan, Kato, Tomoyo Sakata, Li, Fengwu, Teng, Christine H., Gagaring, Kerstin, et al., 2015. Mutations in the P-type cation-transporter ATPase 4, PfATP4, mediate resistance to both aminopyrazole and spiroindolone antimalarials. ACS Chem. Biol. 10 (2), 413–420. https://doi.org/10.1021/cb500616x.

Ghosh, Jimut Kanti, Shaool, Dan, Guillaud, Philippe, Cicéron, Liliane, Mazier, Dominique, Kustanovich, Irina, Shai, Yechiel, Mor, Amram, 1997. Selective cytotoxicity of dermaseptin S3 toward intraerythrocytic Plasmodium falciparum and the underlying molecular basis. J. Biol. Chem. 272 (50), 31609–31616. https://doi.org/10.1074/jbc.272.50.31609.

Gilson, Paul R., Kumarasingha, Rasika, Thompson, Jennifer, Zhang, Xinxin, Penington, Jocelyn Sietsma, Kalhor, Robabeh, Bullen, Hayley E., et al., 2019. A 4-cyano-3-methylisoquinoline inhibitor of Plasmodium falciparum Growth targets the sodium efflux pump PfATP4. Sci. Rep. 9 (1), 1–15. https://doi.org/10.1038/s41598-019-46500-5.

Halgren, Thomas A., 2000. Merck Molecular Force Field. 11, 17, pp. 520–552, 1996.

Hanwell, M.D., Curtis, D.E., Lonie, D.C., Vandermeersch, T., Zurek, E., Hutchison, G.R., 2014. Avogadro: an advanced semantic chemical editor, visualization, and analysis platform. Adv. Math. 262, 476–483. https://doi.org/10.1016/j.aim.2014.05.019.

Harvey, Alan L., 2014. Toxins and drug discovery. Toxicon 92, 193–200. https://doi.org/10.1016/j.toxicon.2014.10.020.

Hassan, Nafisa M., Alhossary, Amr A., Mu, Yuguang, Kwoh, Chee Keong, 2017. Protein-ligand blind docking using QuickVina-W with inter-process spatio-temporal integration. Sci. Rep. 7 (1), 1–13. https://doi.org/10.1038/s41598-017-15571-7.

Iguchi, Tomoki, Yokosuka, Akihito, Tamura, Naoya, Takano, Shingo, Mimaki, Yoshihiro, 2020. Bufadienolide glycosides and bufadienolides from the whole plants of helleborus lividus, and their cytotoxic activity. Phytochemistry 176 (January), 112415. https://doi.org/10.1016/j.phytochem.2020.112415.

Jing, Jing, Ren, Wei C., Chun, Li, Bose, Utpal, Parekh, Harendra S., Wei, Ming Q., 2013. Rapid identification of primary constituents in parotoid gland secretions of the Australian cane toad using HPLC/MS-Q-TOF. Biomed. Chromatogr. 27 (6), 685–687. https://doi.org/10.1002/bmc.2858.

Kagoro, Frank, M., Barnes, Karen I., Marsh, Kevin, Ekapirat, Nattwut, Mercado, Chris EG., Sinha, Ipsita, Humphreys, Georgina, Dhorda, Mehul, Guerin, Philippe J., Maude, Richard J., 2022. Charting the enemy lines - mapping genetic markers of artemisinin resistance in Plasmodium falciparum malaria in Asia: a systematic review. The Lancet Microbes (21), 1–9. https://doi.org/10.1016/S2666-5247(21)00249-4.

King, Glenn F., 2011. Venoms as a platform for human drugs: translating toxins into therapeutics. Expet Opin. Biol. Ther. 11 (11), 1469–1484. https://doi.org/10.1517/14712598.2011.621940.

Kobasa, Theerayot, Talundzic, Eldin, Sug-aram, Rungniran, Boondat, Patcharida, Goldman, Ira F., Lucchi, Naomi W., 2018. Emergence and Spread of Kelch13 Mutations Associated with Artemisinin Resistance in Plasmodium Falciparum Parasites in 12 Thai Provinces from 2007 to 2016, 62, pp. 1–10, 4.

Kolodziejczyk-Czepas, Joanna, Pasiński, Bartłomiej, Ponczek, Michał B., Moniuszko-Szajwaj, Barbara, Kowalczyk, Mariusz, Pecio, Łukasz, Nowak, Paweł, Anna, Stochmal, 2018. Bufadienolides from kalanchoe daigremontiana modulate the enzymatic activity of plasmin - in vitro and in silico analyses. Int. J. Biol. Macromol. 120, 1591–1600. https://doi.org/10.1016/j.ijbiomac.2018.09.143.

Krenn, Liselotte, Kopp, Brigitte, 1998. Bufadienolides from animal and plant sources. Phytochemistry 48 (1), 1–29. https://doi.org/10.1016/S0031-9422(97)00426-3.

Krugliak, M., Feder, R., Zolotarev, V.Y., Gaidukov, L., Dagan, A., Ginsburg, H., Mor, A., 2000. Antimalarial activities of dermaseptin S4 derivatives. Antimicrob. Agents Chemother. 44 (9), 2442–2451. https://doi.org/10.1128/AAC.44.9.2442-2451.2000.

Kückelhaus, Selma, A.S., José Roberto, S A Leite, Muniz-Junqueira, Maria Imaculada, Nonata Sampaio, Raimunda, Bloch, Carlos, Eduardo Tosta, C., 2009. Antiplasmodial and antileishmanial activities of phylloseptin-1, an antimicrobial peptide from the skin secretion of Phyllomedusa Azurea (Amphibia). Exp. Parasitol. 123 (1), 11–16. https://doi.org/10.1016/j.exppara.2009.05.002.

Kumar, Sahil, Bhardwaj, T.R., Prasad, D.N., Singh, Rajesh K., 2018. Drug targets for resistant malaria: historic to future perspectives. Biomed. Pharmacother. 104 (August), 8–27. https://doi.org/10.1016/J.BIOPHA.2018.05.009.

Kwansa-Bentum, Bethel, Agyeman, Kojo, Larbi-Akor, Jeffrey, Anyigba, Claudia, Appiah-Opong, Regina, 2019. *In vitro* assessment of antiplasmodial activity and cytotoxicity of *polyalthia longifolia* leaf extracts on *Plasmodium falciparum* strain NF54. Malaria Res. Treat. 1–9. https://doi.org/10.1155/2019/6976298, 2019 (January).

Laskowski, R.A., MacArthur, M.W., Moss, D.S., Thornton, J.M., 1993. PROCHECK: a program to check the stereochemical quality of protein structures. J. Appl. Crystallogr. 26 (2), 283–291. https://doi.org/10.1107/s0021889892009944.

Liu, Yue, Shi, Daning, Wang, Jin, Chen, Xiaoling, Zhou, Mei, Xi, Xinping, Cheng, Jianming, et al., 2020. A novel Amphibian antimicrobial peptide, phylloseptin-PV1, exhibits effective anti-staphylococcal activity without inducing either hepatic or renal toxicity in mice. Front. Microbiol. 11 (October), 1–14. https://doi.org/10.3389/fmicb.2020.565158.

de Medeiros, Daniel S.S., Rego, Tiago B., De A Santos, Ana P., Pontes, Adriana S., Moreira-dill, Leandro S., Matos, Najla B., Zuliani, Juliana P., et al., 2019. Biochemical and Biological Profile of Parotoid Secretion of the Amazonian Rhinella Marina (Anura : Bufonidae)" 2019.

Oliveira, Gisele Capanema de, Rocha, Sayonarah Carvalho, Miliane Alves da Silva Lopes, Paixão, Natasha, Grego Alves, Silmara Lúcia, Corrêa Pessoa, Marco Túlio, Noël, François, et al., 2021. Implications of synthetic modifications of the cardiotonic steroid lactone ring on cytotoxicity. J. Membr. Biol. 254 (5–6), 487–497. https://doi.org/10.1007/s00232-021-00186-x.

Olliaro, P., 2001. Mode of action and mechanisms of resistance for antimalarial drugs. Pharmacol. Therapeut. 89 (2), 207–219. https://doi.org/10.1016/S0163-7258(00)00115-7.

Pavlovic, Davor, 2014. The role of cardiotonic steroids in the pathogenesis of cardiomyopathy in chronic kidney disease. Nephron Clin. Pract. 128 (1–2), 11–21. https://doi.org/10.1159/000363301.

Pavlovic, Davor, 2020. Endogenous cardiotonic steroids and cardiovascular disease, where to next? Cell Calcium 86, 102156. https://doi.org/10.1016/j.ceca.2019.102156. December 2019.

Phillips, Margaret A., Burrows, Jeremy N., Manyando, Christine, Van Huijsduijnen, Rob Hooft, Van Voorhis, Wesley C., Wells, Timothy N.C., 2017. Malaria. Nat. Rev. Dis. Prim. 3 https://doi.org/10.1038/nrdp.2017.50.

Ramsay, L., Macaulay, M., Degli Ivanissevich, S., MacLean, K., Cardle, L., Fuller, J., Edwards, K.J., et al., 2000. A simple sequence repeat-based linkage map of barley. Genetics 156 (4), 1997–2005. https://doi.org/10.1093/genetics/156.4.1997.

Rieckmann, K.H., Sax, L.J., Campbell, G.H., Mrema, J.E., 1978. Drug sensitivity of Plasmodium: an in-vitro microtechnique. Lancet 22–23.

Rivas, Luis, Juan Román Luque-Ortega, Andreu, David, 2009. Amphibian antimicrobial peptides and Protozoa: lessons from parasites. Biochim. Biophys. Acta Biomembr. 1788 (8), 1570–1581. https://doi.org/10.1016/j.bbamem.2008.11.002.

Rodríguez, Candelario, Rollins-Smith, Louise, Ibáñez, Roberto, Armando, A., Durant-Archibold, Gutiérrez, Marcelino, 2017. Toxins and pharmacologically active compounds from species of the family Bufonidae (Amphibia, Anura). J. Ethnopharmacol. 198, 235–254. https://doi.org/10.1016/j.jep.2016.12.021. July 2016.

Rosling, James E.O., Ridgway, Melanie C., Summers, Robert L., Kirk, Kiaran, Lehane, Adele M., 2018. Biochemical characterization and chemical inhibition of PfATP4-associated Na+-ATPase activity in Plasmodium falciparum membranes. J. Biol. Chem. 293 (34), 13327–13337. https://doi.org/10.1074/jbc.RA118.003640.

Sali, A., Eswar, N., Pieper, U., Marti-Renom, M.A., Madhusudhan, M., Fiser, A., Ilyin, V., 2002. Comparative Protein Structure Modeling of Genes and Genomes, 58, 2002.

Santos, Dos, André Gonzaga, Ferreira, Paulo Michel Pinheiro, Vieira, Gerardo Magela, Perez, Carla Cristina, Tininis, Aristeu Gomes, Silva, Geraldo Humberto, Bolzani, Vanderlan Da Silva, Costa-Lotufo, Letícia Veras, Ó Pessoa, Cláudia Do, Cavalheiro, Alberto José, 2010. Casearin X, its degradation product and other clerodane diterpenes from leaves of casearia sylvestris: evaluation of cytotoxicity against normal and tumor human cells. Chem. Biodivers. 7 (1), 205–215. https://doi.org/10.1002/cbdv.200800342.

Schmeda-hirschmann, Guillermo, Quispe, Cristina, Vargas, Gabriel, 2016. Toxicon Antiproliferative Activity and Chemical Composition of the Venom from the Amazonian Toad Rhinella Marina (Anura : Bufonidae), 121. https://doi.org/10.1016/j.toxicon.2016.09.004, 119–29.

Schoner, Wilhelm, 2002. Endogenous cardiac glycosides, a new class of steroid hormones. Eur. J. Biochem. 269 (10), 2440–2448. https://doi.org/10.1046/j.1432-1033.2002.02911.x.

Shafik, Sarah H., Cobbold, Simon A., Barkat, Kawthar, Richards, Sashika N., Manuel Llinás, Nicole S. Lancaster, Hogg, Simon J., Summers, Robert L., McConville, Malcolm J., Martin, Rowena E., 2020. The natural function of the malaria parasite's chloroquine resistance transporter. Nat. Commun. 11 (1) https://doi.org/10.1038/s41467-020-17781-6.

Shao, Huili, Li, Bingqian, Li, Huan, Gao, Lei, Zhang, Chao, Sheng, Huagang, Zhu, Liqiao, 2022. Novel strategies for solubility and bioavailability enhancement of bufadienolides. Molecules 27. https://doi.org/10.3390/molecules27010051.

Shen, Min-yi, Sali, Andrej, 2006. Statistical potential for assessment and prediction of protein structures. Protein Sci. 15 (11), 2507–2524. https://doi.org/10.1110/ps.062416606.

Spillman, Natalie Jane, Kirk, Kiaran, 2015. The malaria parasite cation ATPase PfATP4 and its role in the mechanism of action of a new arsenal of antimalarial drugs. Int. J. Parasitol.: Drugs Drug Resist. 5 (3), 149–162. https://doi.org/10.1016/j.ijpddr.2015.07.001.

Spillman, Natalie J., Allen, Richard J.W., McNamara, Case W., Yeung, Bryan K.S., Winzeler, Elizabeth A., Diagana, Thierry T., Kirk, Kiaran, 2013. Na+regulation in the malaria parasite Plasmodium falciparum involves the cation ATPase PfATP4 and is a target of the spiroindolone antimalarials. Cell Host Microbe 13 (2), 227–237. https://doi.org/10.1016/j.chom.2012.12.006.

Tai, Hio Kuan, Jusoh, Siti Azma, Siu, Shirley W.I., 2018. Chaos-embedded particle Swarm optimization approach for protein-ligand docking and virtual screening. J. Cheminf. 10 (1), 1–13. https://doi.org/10.1186/s13321-018-0320-9.

Tajuddeen, Nasir, Van Heerden, Fanie R., 2019. Antiplasmodial natural products: an update. Malar. J. 18 (1), 1–62. https://doi.org/10.1186/s12936-019-3026-1.

Tilley, Leann, Judith Straimer, Gnädig, Nina F., Ralph, Stuart A., Fidock, David A., 2016. Artemisinin action and resistance in Plasmodium falciparum. Trends Parasitol. 32 (9), 682–696. https://doi.org/10.1016/j.pt.2016.05.010.

Toyoshima, Chikashi, Kanai, Ryuta, Cornelius, Flemming, 2011. First crystal structures of Na +,K +-ATPase: new light on the oldest ion pump. Structure 19 (12), 1732–1738. https://doi.org/10.1016/j.str.2011.10.016.

Trager, William, 1995. Cultivation of malaria parasites. Methods Cell Biol. 45 (C), 7–26. https://doi.org/10.1016/S0091-679X(08)61844-0.

Trott, O., Olson, A.J., 2012. Software news and update AutoDock Vina: improving the speed and accuracy of docking with a new scoring function, efficient optimization, and multithreading. J. Comput. Chem. 32, 174–182. https://doi.org/10.1002/jcc.

Tu, Youyou, 2011. The discovery of artemisinin (Qinghaosu) and gifts from Chinese medicine. Nat. Med. 17 (10), 1217–1220. https://doi.org/10.1038/nm.2471.

Turner, Helen, 2016. Spiroindolone NITD609 is a novel antimalarial drug that targets the P-type ATPase PfATP4. Future Med. Chem.

Utkin, Yuri N., 2015. Animal venom studies: current benefits and future developments. World J. Biol. Chem. 6 (2), 28. https://doi.org/10.4331/wjbc.v6.i2.28.

Venkatanambi, Kamalakkannan, Salim, Angela A., Capon, Robert J., 2017. Microbiome-mediated biotransformation of cane toad bufagenins. J. Nat. Prod. 80 (7), 2012–2017. https://doi.org/10.1021/acs.jnatprod.7b00134.

Wei, Wen long, An, Ya ling, Zhang, Yan zhi, Li, Zhen wei, Zhou, Yang, Lei, Min, Zhang, Jian qing, et al., 2020. Quantitative analysis of fourteen bufadienolides in venenum bufonis crude drug and its Chinese patent medicines by ultra-high performance liquid chromatography coupled with tandem mass spectrometry. J. Ethnopharmacol. 251 (December 2019), 112490 https://doi.org/10.1016/j.jep.2019.112490.

Wells, Timothy N.C., 2011. Natural products as starting points for future anti-malarial therapies: going back to our roots? Malar. J. 10 (Suppl. 1), 1–12. https://doi.org/10.1186/1475-2875-10-S1-S3.

World Health Orgnization (WHO), 2021. World Malaria Report 2021.

Zhong, Yue, Zhao, Chao, Wu, Wen Yu, Fan, Tian Yuan, Li, Nian Guang, Chen, Min, Duan, Jin Ao, Shi, Zhi Hao, 2020. Total synthesis, chemical modification and structure-activity relationship of bufadienolides. Eur. J. Med. Chem. 189, 112038 https://doi.org/10.1016/j.ejmech.2020.112038.